ORIGINAL PAPER

Realistic flight conditions on ground: new research facility for cabin ventilation

Pascal Lange[1] · Tobias Dehne[1] · Daniel Schmeling[1] · Axel Dannhauer[1] · Ingo Gores[2]

Abstract

A new full-scale test bench was developed and set up at the German Aerospace Center in Göttingen to experimentally analyze novel ventilation approaches for aircraft under realistic thermodynamic boundary conditions. The new ground-based test rig represents a modern twin-aisle cabin layout characteristic for long-haul airliners. In addition to having a realistic cabin geometry, it also facilitates the experimental simulation of thermodynamic boundary conditions to study the performance of alternative ventilation concepts for different flight phases (e.g., climbing or cruising). The implemented fuselage elements as well as the floor are temperature controllable. Using this kind of mantle heating/cooling system allows dynamic changes of inner surface temperatures in a range covering the operationally relevant temperature and time scales. With this experimental set-up, a complete flight scenario (i.e., taxiing, climbing, cruising and descent) can be simulated thermodynamically. Thermal manikins were used during the studies to simulate the passenger's heat impact experimentally. Latest measurement techniques comprising the acquisition of flow velocities, fluid temperatures as well as surface temperatures were used. Based on these data, integral quantities like the mean temperature stratification and mean velocity levels near the manikins, the heat removal efficiency as well as the predicted mean vote and the percentage of dissatisfied passengers were calculated to score the ventilation concepts in terms of passenger comfort for two different operational scenarios under steady boundary conditions.

Abbreviations

CAD	Computer aided design
CAO	Ceiling air outlet
CFD	Computational fluid dynamics
DAC	Digital-analog-converter
$\langle DR \rangle$	Draft rate (averaged) [%]
ECS	Environmental control system
FDL	Flight direction left
FDR	Flight direction right
FL	Flight level
FTF	Flight test facility
GHG	Greenhouse gas
HDoG	Hot-day-on-ground
HRE	Heat removal efficiency [−]
HVAC	Heating ventilation and air conditioning
IATA	International air transport association
IFE	Inflight entertainment
IR	Infrared
LAO	Lateral air outlet
MJV	Micro-jet ventilation
MP	Measurement plane
MV	Mixing ventilation
OVTP	Omnidirectional velocity and temperature probe
PMV	Predicted mean vote [−]
PPD	Predicted percentage dissatisfied [%]
Qv	Flow rate [l/s]
RTD	Resistance temperature detector
SR	Sensor rack
T_{aisle}	Fluid temperature in the aisle [°C]
T_{cab}	Mean cabin temperature [°C]

✉ Pascal Lange
pascal.lange@dlr.de

1 German Aerospace Center (DLR), Institute of Aerodynamics and Flow Technology, Bunsenstraße 10, 37073 Göttingen, Germany

2 Airbus Operations GmbH, Kreetslag 10, 21129 Hamburg, Germany

$\langle T \rangle_{chest}$	Fluid temperature (averaged) near the manikins
$\Delta \langle T \rangle_{chest}$	Gradient between max. and min. $\langle T \rangle_{chest}$ [K]
T_{gap}	Gap temperature [°C]
ΔT_{h-a}	Gradient between head and ankle temp. [K]
T_{in}	Supply air temperature [°C]
TM	Thermal manikin
T_{out}	Exhaust air temperature [°C]
T_{surf}	Surface temperature [°C]
$\langle U \rangle$	Fluid velocity (averaged) [m/s]

1 Introduction

To address the global challenge of climate change and their actions to limit global warming, a significant reduction in Greenhouse Gas (GHG) emissions from all sectors of economy is mandatory. Within this context, the commercial aviation industry is faced with quantitative goals for limiting GHG, which were set by different institutions and stakeholders. The targets most likely to become prominent for the aviation sector were published by the International Air Transport Association (IATA) in 2009 and are related to the optimization of the energy efficiency associated with the reduction of carbon dioxide (CO_2) emissions caused by the global aircraft fleet. Specifically, a major goal is to reduce the global fleet's CO_2 emission rate by 50% until 2050, relative to 2005 levels [1]. Further, the recently presented European Green Deal [2] aims for a 90% reduction in transport emission by 2050 (related to 1990-levels). Consequently, the aviation sector has to contribute to the reduction. Hence, technical innovations on all design levels of an aircraft are required and indispensable to meet the challenging goals of decarbonising the global civil aviation.

In addition to the energy consumption through propulsion, the Environmental Control System (ECS) is the most energy-demanding subsystem of passenger aircraft and therefore responsible for the largest extra consumption of fuel. During cruise, up to 75% of non-propulsive power is needed to provide conditioned air to the passenger cabin [3]. While the air conditioning, in terms of cooling and pressurizing the air, consumes a large proportion of the mentioned energy, the ventilation and air distribution system also provides potential to optimize the energy management system of an aircraft ECS. Here, the general trend of rising heat loads in modern passenger cabins, characterized by an increased installation of Inflight Entertainment (IFE), new power sources (e.g., modular autonomous galley with integrated power cell) [4] and higher passenger densities, promote the interest of the aircraft industry in alternative ventilation concepts which support an efficient fresh air supply. Simultaneously, novel ventilation concepts might provide further benefits like an improved thermal passenger comfort,

a higher air quality level as well as the opportunity to reconsider the cabin layout and thus help to improve industrial and manufacturing processes economically. Regarding new cabin layouts, aircraft manufacturers have a great interest to simplify the process of customizing aircraft cabin design and architecture, especially for large commercial aircraft [5]. The approach of modularizing the cabin interior offers airlines possibilities to create a new level of flight experience [6] and thus improved customer satisfaction. From the manufacturer's point of view, the modular design approach provides advantages to improve and simplify manufacturing processes using preassembled and swappable cabin modules, which is an important technology component for advanced aircraft manufacturing. The engineering and subsystems, such as electrical, oxygen and even the ventilation systems (e.g., ducting, cabin air inlets, etc.), need to be installed in the modules. In that sense, novel ventilation concepts are suitable for the modular aircraft cabin design approach if the integrability in single modules of the cabin is considered during the development phase. Thus, novel ventilation concepts provide the opportunity for redesigning and rethinking the cabin layout and cabin structure including the ducting system as well as the air inlet and exhaust openings to facilitate a higher level of prefabrications during the manufacturing process of an aircraft.

The aforementioned facts justify the need for new and alternative ventilation concepts, which promise energy and weight-saving potential along with similar or even enhanced thermal passenger comfort, air quality level as well as advantages regarding more efficient manufacturing processes. To analyze and evaluate new ventilation concepts, two methods are common, which were used either separately but rather simultaneously to calibrate and validate the methods with each other. In that sense, the work of Elmaghraby et al. [7] gives a comprehensive overview of the research activities in the last two decades addressing the aircraft ventilation using experimental and numerical methods. The latter are simulation tools for studying novel ventilation approaches in detail [8–10]. Generally, computational fluid dynamics (CFD) simulations are used to calculate resulting fluid and surface temperatures, flow velocities, turbulence intensities as well as ventilation efficiencies and pollutant dispersal by means of steady and unsteady computational simulation methods. In addition, experimental studies are conducted to analyze novel ventilation scenarios. Here, it is crucial to simulate realistic boundary conditions, both geometrically as well as thermodynamically, to cover all relevant flight scenarios and operational phases. Therefore, flight tests are considered to be the most appropriate experimental scenario to verify and validate novel concepts under realistic stationary as well as non-stationary boundary conditions [11, 12]. Especially the work of [13] prove, that different thermodynamic boundary conditions occur (e.g., temperatures

of the cabin's inner surfaces) dependent on the flight and operational phase. However, flight tests are quite costly and time consuming due to the necessary detailed and protracted planning before, including the flight certification requirements for the measurement equipment. Hence, the applicable measurement systems within an aircraft cabin during a flight scenario are limited. Further, the test scenario is limited to existing and available air plane geometries. Due to the economic considerations, experimental investigations of studies regarding cabin indoor air environments are usually conducted on dedicated test benches at ground level. However, some available studies were only focused on cabin layouts characterized by single-aisle configurations [14, 15]. Twin-aisle cabin layouts were considered by experimental studies in a cabin mock-up based on a 767–300 section [16, 17]. Further test benches, providing a twin-aisle layout, are described in [18] and [19]. The latter work provides information about experimental studies in a five-row section of a MD-82. However, the aforementioned studies focusing on long-range airliner mock-ups were conducted in highly simplified environments (i.e., very short cabin sections) in contrast to real aircraft cabins, which hardly allow for conclusions to operational scenarios. Further, there are no studies published so far, which address the performance of novel ventilation concepts for commercial long-range airliners under non-stationary or non-ideal boundary conditions. To the knowledge of the authors, the single-aisle mock-up section at Tianjin University [20, 21] and the twin-aisle Flight Test Facility (FTF) at the Fraunhofer-Institute in Germany [22] are the only test benches mentioned in the scientific literature, facilitating a static temperature control of the sidewalls and fuselage respectively. The FTF is also installed within a low-pressure vessel to simulate the air pressure conditions during a flight experimentally. However, information on whether dynamic changes of the thermodynamic boundary conditions in a range covering relevant temperature and time scales are possible is still lacking for both test rigs. Further, the mentioned test rigs are geometrically limited by the defined outer shell and thus not adjustable to other aircraft geometries and configurations, which is mandatory to evaluate the performance of novel ventilation modes holistically under realistic conditions in time and cost-efficient test sequences. Certainly, the leading aircraft manufacturers (e.g., Airbus, Boeing) also operate some test facilities, which probably provide the technical features to simulate different flight scenarios experimentally. Unfortunately, however, publicly available data are not found in the literature.

The aim of the present work is twofold. Firstly, a new full-scale, long-range aircraft cabin mock-up for testing alternative air distribution systems under static and dynamic boundary conditions is introduced. It enables the installation of different cabin geometries and provides the flexible integration of novel ventilation concepts. In addition, it

facilitates thermodynamically realistic boundary conditions to simulate different flight phases in operationally relevant temperature and time scales. Here, besides the simulation of different flight phases under steady conditions, dynamic effects and non-ideal thermodynamic boundary conditions can also be simulated. A feasibility study was conducted by simulating an entire flight scenario and compare it with data acquired during flight tests. In the second part of the study, a new cabin ventilation approach is analyzed in terms of thermal passenger comfort and efficiency, experimentally. Here, the studies are focused on two different operational scenarios characterized by the experimental simulation of a cruising phase and a Hot-Day-on-Ground (HDoG) scenario, representing an aircraft on ground at very warm ambient temperatures, e.g., waiting for departure. To evaluate the performance of the novel ventilation approach, the results are compared with a reference scenario based on a generic mixing ventilation system.

2 New cabin mock-up and test environment

2.1 General description and cabin layout

The new modular cabin mock-up (in German: "Modulares Kabinen Mock-Up Göttingen"—MKG) [23] of the German Aerospace Center (DLR) in Göttingen was developed, set up and chosen as a test platform for the presented studies. It is a test bed for aircraft cabin research activities at ground level representing a full-size (1:1 scale) cabin section of modern wide-body airliners in the current expansion stage. Figure 1 depicts the inner view of the cabin. The inner dimensions comprise a total length of L = 9.96 m, a width of W = 6.25 m as well as a height of H = 2.7 m.

For the investigation of novel ventilation systems for aircraft, it is crucial for the experiments to provide geometric similarity to real aircraft cabins. Therefore, the entire interior paneling (e.g., sidewalls, lateral and center overhead
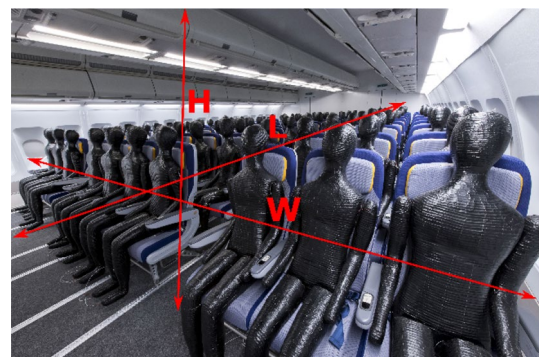
Fig. 1 Inner view of the mock-up showing cabin layout with real aircraft seats arranged in a typical twin-aisle configuration

bins, ceiling panels as well as dado panels) are realized using second-hand aircraft parts. Further, the seats are also second-hand, to realize a realistic seating arrangement, see Fig. 1. A twin-aisle layout is realized, characterized by a 10-abreast seating configuration arranged in a 3-4-3 seating layout. During the studies, economy seating class is implemented only. However, the installation of different seating classes, i.e., business, first or economy plus is also feasible. The baseline layout provides 10 seat rows with a 32" seat pitch. Hence, the cabin offers space for 100 passengers in total.

To study a wide range of promising ventilation scenarios in any existing or planned cabin geometry, the new test rig was designed on the premise to provide the best possible modularity. This includes the integration and operation of different air distribution systems with a high degree of flexibility addressing the implementation of a multitude of air supply and exhaust configurations within the cabin. Additionally, for upcoming projects the test rig should not be limited to long-range cabin layouts only, but rather to any type of airliners, such as short- or medium-range aircraft or even to alternative concepts (i.e., flying wings) or other ventilated passenger compartments in general. To support the first point of modularity, the cabin structure provides areas to integrate new types of cabin air inlets as well as cabin air exhaust modules with manageable effort. Here, easily replaceable facing elements above and under the overhead bins, in the ceiling as well as at floor level are considered. Figure 2a gives an overview of the possible air supply and exhaust positions, which can be implemented in the mock-up structure. The blue arrows indicate the air supply while the red highlighted arrows are referred as air exhaust.

The second feature regarding the investigation of different cabin cross sections is achieved using an external framework as a support structure for the installation of the interior cabin parts. The support structure enables the flexible installation of individual cabin parts. The fastening method facilitates a flexible moving and adjusting of brackets, which keep the cabin's interior panels in position. Subsequently different

cabin geometries can be installed replacing the linings through other fuselage elements at the mounting positions. Figure 2b schematically illustrates the installation of different cabin geometries in the support structure. Here, the black highlighted contour represents a large twin-aisle cabin while a smaller single-aisle cabin is colored in light gray. The flexible mounting system is represented by red arrows.

2.2 Thermodynamic boundary conditions

As indicated in the introduction, it is important to evaluate the performance of novel ventilation concepts under realistic thermodynamic boundary conditions. In addition to the realistic simulation of thermal loads, i.e., passengers, this also includes the static and dynamic simulation of different operational phases that occur during a typical flight scenario (e.g., hot-day-on-ground, climb, cruise). The surface temperature distribution of the cabin's interior lining is different dependent on the flight phase. This phenomenon was monitored and acquired by measurements of the interior surface temperatures during various flight tests carried out with the DLR's test aircraft ATRA, which is an Airbus A320-232 [13]. This needs to be considered to evaluate novel ventilation approaches in terms of energy efficiency, thermal passenger comfort and air quality. According to internal communication and data from previous flight tests in the DLR A320 ATRA [13, 24], the air temperature located in the gap between the primary and secondary insulation of a typical aircraft fuselage varied in a range of 10 °C to 35 °C depending on the flight phase (e.g., cruise or HDoG). Based on this knowledge, the fuselage elements of the new cabin are temperature-controlled to simulate the gap temperature experimentally. However, to simulate realistic surface temperature distributions at the inner linings using this technical approach, it is crucial to take the right heat transfer coefficients into account. Hence, real interior lining parts of an Airbus A340 are installed, which comprise original secondary insulation packages, see Fig. 3a. Furthermore, a recent study [25] showed the impact of different insulation

| (a) | (b) |
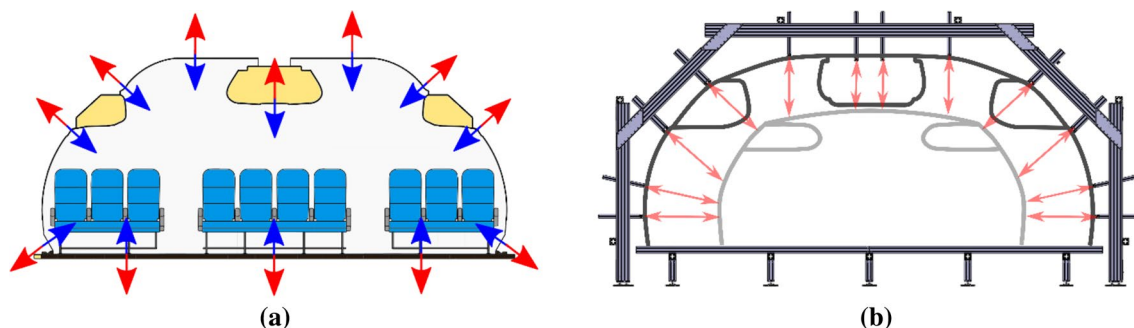
Fig. 2 Modularity of the new facility. **a** Schematic illustration of possible air supply and exhaust configurations. **b** Sketch regarding the implementation of different cabin geometries
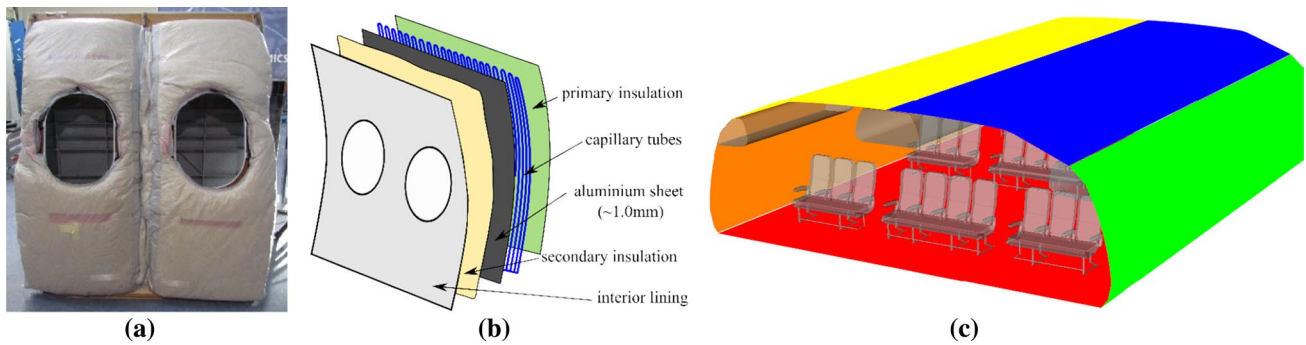
Fig. 3 Temperature-controlled fuselage elements. **a** Original aviation insulation package (secondary) attached at the back of the sidewall panel. **b** Schematic set-up of a temperature-controlled lining part using the example of a sidewall panel. **c** Individually controllable cabin zones indicated by a different color mapping

materials on the gap temperature, the condensation behavior and the surface temperature of the linings highlighting the importance of well fitted insulation packs.

The technical approach to implement a temperature control system at the fuselage elements is based on capillary tubes, which are floated through by a water glycol mixture at a defined temperature level. As schematically shown in Fig. 3b, the capillary mats are mounted on aluminum sheets and are attached at the back of the lining elements. The capillary tubes are characterized by large volume flows but comparatively small tube diameters. The close-spacing capillaries in combination with the aluminum sheets ensure a homogeneous temperature distribution behind the interior lining to simulate the gap temperature. The temperature control system is subsequently covered by an insulation layer with a thickness of 50 mm, representing the primary insulation of an aircraft, however, needed here to reduce thermal losses to the test hall. All the installed interior parts, comprising the dado, sidewall and ceiling panels as well as the overhead bins and even the floor, are equipped with the specified temperature control system. The front and rear side of the cabin mock-up is not temperature-controlled and kept under adiabatic thermal conditions using sufficiently thick insulation. By operating five different temperature control units, the cabin's fuselage can be controlled individually in corresponding zones. Figure 3b indicates, with the help of a CAD rendering, the individual controllable cabin zones comprising the floor, both (left and right) sidewalls and lateral overhead bins as well as both ceiling zones.

Thanks to the usage of second-hand aircraft lining elements with original insulation layer, realistic thermal characteristics, such as thermal conductivity and heat transfer coefficients, are considered. As a result, realistic surface temperature distributions at the inner linings can be experimentally simulated for different operational phases. For optimal adjustment and monitoring of the gap temperature, over 50 resistance temperature detectors (RTD) are installed on the aluminum sheets distributed along the temperature controllable zones of the cabin's fuselage.

2.3 Experimental simulation of dynamic situations

Results of tests regarding dynamic changes of the thermodynamic boundary conditions are shown in Fig. 4. To validate the temperature control system, temperature data in the gap measured during flight tests with the DLR-ATRA [24] serves as a reference case for the experimental simulation (see top graph of Fig. 4). Both graphs in Fig. 4 show spatially averaged temperature data. The test scenario comprises the simulation of an entire flight schedule including take-off, climb, cruise, decent and landing phase. As shown in the top graph, the gap temperature of the DLR-ATRA is around 22 °C before take-off. Here, the aircraft was prepared for flight including taxi-out.
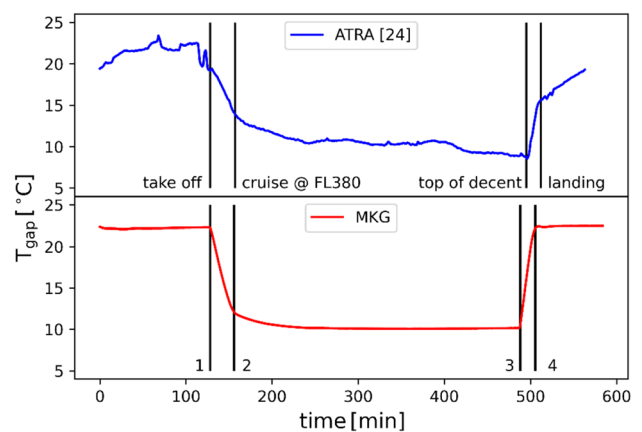
Fig. 4 Dynamic change of thermodynamic boundary conditions (spatially averages temperatures) representing the operational phases of a flight. Top: gap temperature (blue) measured during flight tests [24]. Bottom: gap temperature (red) experimentally simulated with the temperature-control-system of the new mock-up

The take-off was at a time of 128 min and the climbing phase starts. At this point, the gap temperature starts to decrease rapidly. Cruising altitude was reached after another 30 min characterized by a temperature drop of 6.5 K (between take-off and cruise level). During cruise at flight level FL 380, the gap temperature decreases gradually to a value of less than 10 °C. The top of decent was reached at a time of 495 min and the landing was completed at 515 min. In this period of time, the gap temperature increases by 7.0 K. Afterwards the gap temperature continues to rise. These temperature data are the benchmark to test and validate the temperature control system installed in the new cabin test facility. Hereto, we reproduce the temperature profile experimentally in the bottom graph of Fig. 4, representing the gap temperature of the temperature-controlled fuselage elements. Here, the mentioned flight phases are denoted with numbers from 1 to 4. According to the flight test data, the temperature control system was set to 22 °C. After about two hours, the take-off was simulated by adjusting the set temperature to 10 °C (see number 1 at the bottom graph). After exactly the same period of time as marked in the blue graph, the gap temperature of the mock-up decreases by 8.9 K, which is slightly higher compared to the flight test data. The set point of 10 °C was reached after roughly two hours, which is comparable with the temperature profile measured during tests with the DLR-ATRA. At number 3, the operational phase of decent was simulated experimentally by adjusting the gap temperature back to the initial value of 22 °C. The black vertical line marked with number 4 represents an equal time range as shown in the blue graph. In this period, the temperature rises to 21.7 °C. The gradient of almost 12 K (from 10 °C to 21.7 °C) is significantly larger than the temperature gradient occurred under real conditions and might be adjusted in upcoming tests in the cabin mock-up. Additionally, it should be noted, that the temperature homogeneity over the aluminum sheets with a maximum difference of only 2.0 K was realized. In summary, the validation test has proven that even dynamic effects by changing the thermodynamic boundary conditions can be simulated in realistic temperature and time scales to simulate different flight phases experimentally. In addition, the effects due to the angle of attack of the aircraft e.g., during climb, or influences because of an accelerating aircraft are not considered in our test rig. However, in specific with regard to air movement within the cabin and the spread of airborne diseases, recent studies [26] showed a small but existing impact on the spreading behavior of contaminants at normal aircraft accelerations. Thus, this point should be considered when transferring our results from the 10 m cabin mock-up to a full-length aircraft.

2.4 Air conditioning and ventilation system

The test rig is powered by a sophisticated Heating, Ventilation and Air Conditioning (HVAC) system to supply the cabin with the necessary amount of chilled air. The HVAC meet the requirements in terms of thermodynamic parameters and volume flow rates for an aircraft cabin occupied with 100 passengers. Hence, volume flow rates of at least 1000 l/s as well as cabin inlet temperatures between 10 °C and 55 °C are possible. Besides the supply of pure chilled fresh air, the system also allows the use of recirculated air in a desired splitting level by opening of the recirculation valve. This benefit both the reduction of the cooling demand of the HVAC and experimental studies addressing the air quality level since the simulation of realistic distribution ways for air pollutions or tracer gasses (e.g., CO_2 of SF_6) is ensured. Volume flow control of the supply air was realized by 36 individually monitored and controlled supply pipes, each of them equipped with a venturi nozzle, a Sensirion SDP800 differential pressure probe [27] and a HVAC valve. During calibration tests, the volume flow control system provides accuracies of about 1.5%. A control algorithm calculates a proposed voltage, which is subsequently sent to the valve controller by means of a Digital-to-Analog Converter (DAC) to set the valve position. This set-up ensures an efficient, homogeneous and accurate distribution of the inlet mass flow and additionally allows an individual variation of the incoming volume flow and precise flow measurements simultaneously.

For the present study, a micro-jet ventilation (MJV) scenario was investigated. This ventilation approach represents a state-of-the-art concept for trains, which is often used during cooling scenarios [28]. It is characterized by a high degree of mixing with jets of fresh air entering the cabin in the aisle at ceiling level, see Fig. 5a. A perforated ceiling brings the air into the passenger compartment as localized micro-jets with a rather high momentum. The installed MJV air outlets consist of holes with a diameter of 3 mm at a lateral spacing of 20 mm in each direction. As indicated in Fig. 5a, the exhaust air openings are located in the lower part of the cabin, on both sides right above the floor, corresponding to the position of the Dado panels. Additionally, as benchmark case, a generic mixing ventilation (MV), which is state-of-the-art in aircraft cabins, was installed with lateral and ceiling air outlets (LAO and CAO) as well as exhaust through the Dado panels, see Fig. 5b.

In this work, two different operational phases were simulated experimentally by means of the temperature-controlled fuselage elements described in Sect. 2.2. The two simulated thermodynamic boundary conditions are summarized in Table 1. The main focus of interest is the "cruise" case with cold gap temperatures. Here, the measurement techniques
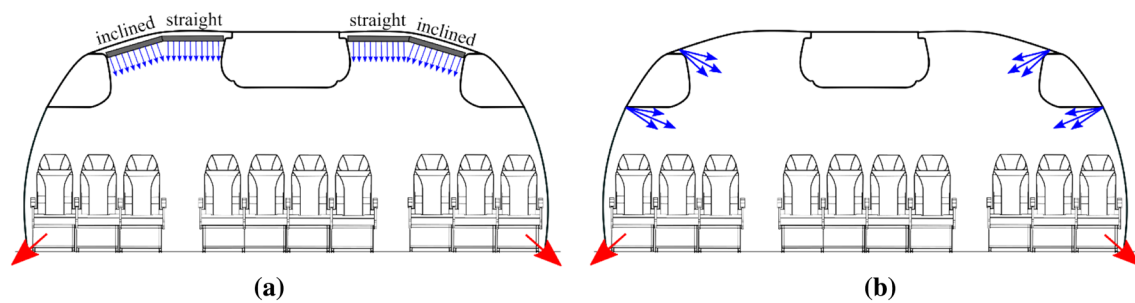
Fig. 5 Sketch of the studied ventilation scenarios where blue arrows denote the supply air and red arrows illustrates the exhaust air for **a** MJV and **b** MV

Table 1 Characteristics of studied operational phases

Operational phase	Typical boundary conditions	Main challenges for ventilation system
Cruise	• Typical flight condition • Low temperatures in the gap between primary and secondary insulation	• Main operational mode • Efficient operation of entire HVAC system • Long-term comfortable conditions for passengers
Hot day on ground	• Waiting for departure/take-off, e.g., in Dubai • High temperatures in the gap between primary and secondary insulation	• Highest cooling demand for HVAC • Varying thermal loads during boarding • Efficient removal of heat loads • Providing acceptable conditions for passengers

are used to characterize the benefits and drawbacks of MJV under static conditions at 'cruise' flight level compared to the generic MV ventilation. Furthermore, the scenario "Hot Day on Ground", where the cooling-down process of the warm cabin after the boarding procedure with a fully occupied cabin was simulated.
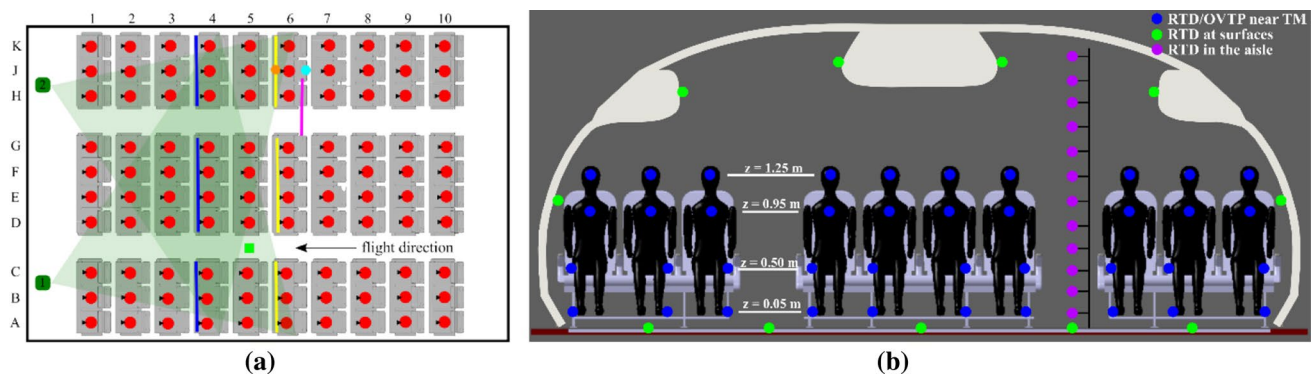
2.5 Thermal Manikins

To ensure realistic heat loads and obstruction, which are important for the generation of buoyancy forces and dissipation of momentum, thermal manikins (TMs) were used during the experimental studies. Each TM can be heated individually by an external power supply to provide a constant sensible heat release in a range of 0 to 150 W. A main benefit of the TMs is the very homogeneous exhibition of heat flux density, which is slightly increased in the head region reproducing real human. The homogeneous distribution of the heat load over the manikin's surface is crucial to accomplish realistic surface temperatures and thus buoyancy forces. For this study, an automatic control of the heat release depending on the mean temperature in the cabin was set. The automatic mode provides a more realistic simulation of the human metabolism, i.e., the warmer the environment, the less sensible heat is released by the humans. The underlying heat release – cabin temperature curve is based on a

standard [29]. The TMs placed within the cabin are shown in Fig. 1.

3 Measurement techniques

This section provides an overview of the installed measurement techniques used to determine comfort relevant quantities as well as key figures to analyze the energy efficiency of the ventilation approach. In addition to the 100 TMs, the cabin measurement installation basically comprises three sensor racks (SR), a measurement plane (MP) for studying the resulting flow patterns quantitatively and an infrared camera set-up to analyze the surfaces temperature distribution at the TMs as well as at the inner lining elements. In total, more than 250 sensors were installed in the cabin. The positions of the probes capturing fluid and surface temperatures, fluid velocities as well as comfort parameters are described in Sect. 3.1. The latter is followed by a brief specification of the used infrared cameras. The Sect. 3.3 introduces the considered measurement quantities. Here, the limits of the corresponding quantities are also given which serve as evaluation criteria to judge the achievable thermal comfort level as well as the energy efficiency of the ventilation approaches under the two different studied boundary conditions.

(a)   **(b)**

Fig. 6 Cabin layout and measurement installation. **a** Top view with thermal manikins (●) including chest temperature probes (▶). SR1-3 denote the position of the respective sensor racks for temperature SR1 (━), temperature and velocity SR2 (━) and aisle temperatures (■). MP1 (━) depicts the measurement plane for the flow visualization. Further the position of the infrared cameras (■) and the comfort measurements, operative temperature (⬠) and humidity (⬠) are given. **b** Cross-section view. Positioning of RTD and OVTP probes near the TM (blue circles, ●) mounted at SR1 and SR2 in seat row 4 and 6, respectively. Further, probe positioning at SR3 (red circles, ●) to capture fluid temperatures in the aisle as well as probes (green circles, ●) for measuring inner surface temperatures

Figure 6a illustrates the cabin layout including the location of the corresponding measurement installation. Reference is often made to this graphic in the upcoming sections, where the used measurement techniques are characterized.

3.1 Local probes

To capture temperature stratifications near the TMs, a sensor rack (see SR1 in Fig. 6a), equipped with RTDs at four different height levels, were installed in a complete seat row. Figure 6b shows the measurement rack for seat row four, schematically. Here, the sensor's placement at the different heights is specified, while each sensor in the vicinity of the TMs is placed in a distance of 5 cm from the manikin's surface. This distance is close enough to capture the comfort-relevant fluid temperatures next to the TMs without being influenced by the thermal boundary layer caused by the heated TM. A further rack with RTDs mounted at 12 different height levels (illustrated with red dots in Fig. 6b was positioned in the aisle section of seat row five to evaluate temperature stratification in the aisle, see SR3 in Fig. 6a. Moreover, for the acquisition of the temperature homogeneity in the entire passenger cabin, temperature probes were installed at chest level in front of all TMs, see black triangles in Fig. 6a. Surface temperatures were also acquired using 11 RTDs. The latter were installed in a cross section located in the middle of the cabin – aligned with the fifth seat row – as illustrated with green points in Fig. 6b. Combined omnidirectional velocity and temperature probes (OVTP) are used to measure flow velocities and temperatures close to the TMs in a further seat row. Hereto, the sensor rack SR2 (see Fig. 6a) was installed, where the sensor positioning is similar to SR1 with probes at four different heights (at ankle, knee, chest and head level), see blue points in Fig. 6b. Each of the

40 installed OVTP provide an accuracy of ± 0.02 m/s for the velocity and ± 0.2 K for the temperature. As illustrated by cyan and orange hexagons in Fig. 6a, the lately described SR2 was extended and combined with a humidity and an operative temperature probe to determine thermal passenger comfort quantities, such as Predicted Mean Vote (PMV) and Predicted Percentage Dissatisfied (PPD).

In summary, more than 250 local probes are installed at multiple locations to capture comfort-relevant quantities.

3.2 Infrared thermography

Pictures of the inner surface temperatures were recorded using two infrared (IR) cameras, which were installed in the front area of the mock-up. The specific installation position of the cameras and the corresponding field of views are depicted in Fig. 6a with dark green colored squares and areas. Herewith, the surface temperature distribution of the TMs as well as of the interior parts (e.g., seats, overhead bins, panels and air inlets) can be analyzed. Each of the mentioned IR cameras provide a resolution of 640×480 px and a sensitivity of 0.075 K for a temperature range of -20 to 900 °C. In addition to the permanently installed cameras, a further IR camera was used to study the spatial surface temperature distribution of the sidewall panels under stationary boundary conditions. This camera also provides thermal high-resolution images (640×480 px) accompanying with a sensitivity of 0.08 K in a temperature range between -40 and 1200 °C.

3.3 Evaluation parameters

Appropriate evaluation parameters were measured and calculated by means of the data gathered with the used

Table 2 Evaluation parameters with measuring declaration

Parameter	Declaration of measuring
$\langle T \rangle_{chest}$	Time averaged (1800s) temperatures on chest level for 80 RTDs – one for each TM in rows 2 to 9
$\Delta \langle T \rangle_{chest}$	Temperature difference between maximum and minimum value at chest level (of 80 RTDs)
ΔT_{h-a}	Local temperature difference between head and ankle at SR1, calculated for each seat position in seat row 4
T_{aisle}	Temperatures measured with SR3 in the aisle section at 12 height levels
T_{sur}	Surface temperatures measured with infrared thermography
$\langle U \rangle$	Velocity measured at SR2 (row 6) for 10 seats at ankle, knee, chest and head position
$\langle DR \rangle$	Mean draft rate (spatially averaged over all seats and all heights) measured at SR2
HRE	Heat removal efficiency calculated with T_{in}, T_{out}, T_{cab}
PMV	Predicted mean vote
PPD	Predicted percentage of dissatisfied people

measurement systems. Table 2 summarizes the considered evaluation parameters and briefly describes the measuring and calculation methodology, respectively.

As described in Sect. 3.1, the temperatures in the vicinity of the TMs were measured at different height levels for SR1 and at chest level in front of all TMs. The corresponding data are used to evaluate thermal passenger comfort by means of the occurred temperature differences between head and ankle (ΔT_{h-a}) as well as between the maximum and minimum values of the temperatures measured at chest level ($\Delta \langle T \rangle_{chest}$). In addition, fluid temperatures in the aisle (T_{aisle}) as well as surface temperatures (T_{sur}) at the lining elements are part of the temperature data evaluation. Besides local temperature values, the flow velocities $\langle U \rangle$ in the passenger zone are an important measure to evaluate passenger comfort for a specific ventilation approach. The data recorded by local probes installed at SR2 are used to prove whether comfort-critical velocities occurred and hence a draft risk (DR) is present. The DR is also acquired by the sensors at SR2 and considered during the data analysis. Further, parameters addressing the thermal passenger comfort were analyzed using the PMV and the PPD. Both values represent integral thermal comfort quantities comprising air temperature, radiation temperature, air velocity as well as air humidity.

Additionally, the heat removal efficiency (HRE) is considered, which is a commonly used parameter to evaluate the efficiency of a ventilation system. Here, higher HRE values represent a more efficient removal of the heat.

The gap temperature (T_{gap}) is recorded simultaneously for adjusting and monitoring the thermodynamic boundary conditions. The two presented scenarios in this work are characterized by a gap temperature of approximately 10.0 °C for the cruise conditions and 35.0 °C for the HDoG scenario. Generally, for the sake of comparability and to simulate the ECS scenario of an airplane

as realistically as possible, the cabin temperature of $T_{cab} = 23$ °C serves as a setpoint and a control temperature for all investigated cases. To reach the corresponding T_{cab} and keep them constant, the air supply temperature (T_{in}) was adjusted individually for the studied cases.

4 Results

To demonstrate the operational readiness and the capabilities of the new facility, the two aforementioned ventilation configurations were installed and analyzed experimentally initially with baseline tests. A volume flow rate of $Qv = 1000$ l/s, i.e., a flow rate of 10 l/s per passenger, was set. In the first stage, two different stationary thermodynamic boundary conditions were studied for MV and MJV, the cruise case and the HDoG scenario. Thereby, the presented manuscript focuses on the feasibility of the new cabin mock-up to investigate novel ventilation approaches for aircraft and its readiness for further investigations.

The results chapter is divided into six sections starting with a qualitative analysis of the resulting flow patterns using laser-smoke visualizations, see Sect. 4.1. Section 4.2 shows the mean fluid and the surface temperature evaluation followed by the fluid velocities at four height levels in SR2 in Sect. 4.3. Subsequently, the HRE values are presented and discussed in Sect. 4.4 followed by the results of the comfort-relevant parameters PMV and PPD. Finally, the results are scored addressing the thermal passenger comfort using previously defined criteria and limitations. The scoring is visualized by means of color coding based on the traffic light color scheme.

Table 3 summarizes the boundary conditions for the studied cruise and HDoG scenario of MJV and MV, respectively. With a specified cabin mean temperature of $T_{cab} = 23$ °C, measured at ten seat positions at four height levels in SR1 (see Fig. 6a, the air supply temperature was

Table 3 Boundary conditions for investigated test cases

Case	Q_v [l/s]	Inclined [l/s]	Straight [l/s]	Ceiling [l/s]	Lateral [l/s]	T_{in} [°C]	T_{out} [°C]	T_{cab} [°C]	T_{gap} [°C]
MJV Cruise	1000	500	500	–	–	18.0	20.8	22.9	10.5
MJV HDoG						12.4	22.5	23.1	35.1
MV Cruise		–	–	600	400	18.2	21.0	23.0	10.6
MV HDoG						13.1	22.9	23.1	34.8

controlled to 18.0 °C and 18.2 °C for the cruise case characterized by $T_{gap} = 10.5$ °C and 10.6 °C, for MJV and MV respectively. For the HDoG scenario, the inlet temperatures were acquired at 12.4 °C and 13.1 °C, while the gap temperatures amounted to $T_{gap} = 35.1$ °C and 34.8 °C, for MJV and MV respectively. Deviations of T_{cab} as small as ± 0.1 K reflecting the high precision of the temperature control system. Further, the gap temperatures were also within a range of ± 0.2 K for each case, highlighting the reproducibility of the facilities boundary conditions.

4.1 Flow visualization

Visualizations of the cabin air flow were created by emission of fog upstream to the cabin air inlets in the measurement plane MP1, see Fig. 6a. Figure 7a and b show the resulting flow pattern of the MJV scenario for cruise and HDoG conditions, respectively. For both conditions, the fresh air supply of the MJV inlets is combined to a downwards flow between the lateral and center overhead bin heading toward the central seats. At MJV for cruise (see Fig. 7a), the fresh air flows first to the TM sitting in the middle row next to the aisle (seat G in FDR), before spreading toward the sides above the ground. Under "HDoG" conditions, the flow was influenced by heat buoyancy due to the warm inner lateral and floor surfaces, see Fig. 7b. The air from the inclined supply flows inbound due to the increased thermal loads on the side. Afterwards, the air descends in the aisle where a part of it hits the shoulder of the TM sitting at seat position G. The higher side-located heat loads of the HDoG scenario result globally in a straighter downward flow. Since T_{in} is significantly lower for the HDoG scenario compared to the cruise case, the incoming jets detach earlier from the surfaces and thus supports the downward directed flow in the aisle.

At MV, the fresh air enters the cabin through inlets above and below the lateral overhead bins, see Fig. 7c and d. For
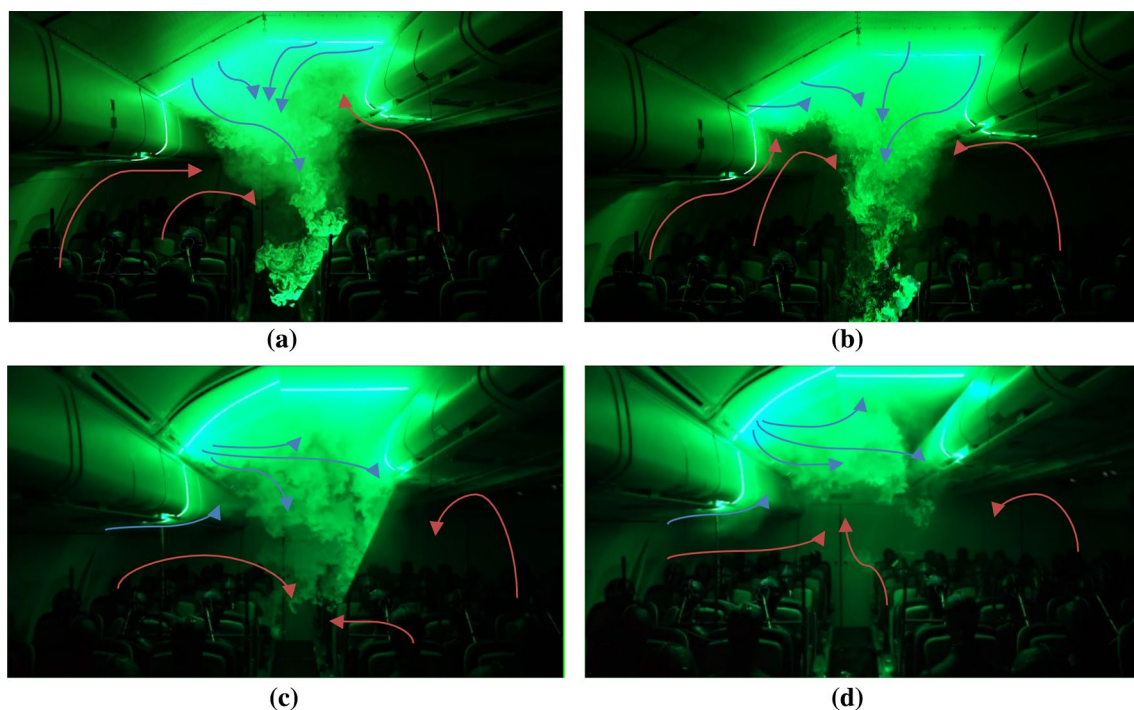

Fig. 7 Flow visualization in the aisle at MP1. **a** MJV for cruising conditions. **b** MJV for HDoG conditions. **c** MV for cruising conditions. **d** MV for HDoG conditions

both conditions (cruise and HDoG), the air jets coming from the ceiling hits the center overhead bin, while the lateral air jets follow the contour of the corresponding lateral overhead bin. During cruise conditions, the major part of the fresh air flows toward the middle of the cabin, whereas a smaller part of the air flows downwards the aisle. After recirculation, the air passes the passengers located at the seat bench near the windows. For the HDoG scenario, the fresh air accumulates between the overhead bins. The high momentum and the additional heat loads caused by the warm fuselage elements induces a vortex structure in the aisle, right beyond the overhead bin. Hence, the air passes the passengers near the aisle before flowing to the TMs near the sidewalls and in the middle of the cabin.

4.2 Temperature measurements

Figure 8 shows the chest temperatures in the vicinity of the TMs as contour plots in top view. The showed data are time-averaged over 1800s. In the first and the last seat row significantly lower temperatures of about 2.5 K occurred in contrast to the remaining seat rows. The reason for this are boundary effects caused by missing heat loads in front of the first and behind the last row. Hence, the first and last seat row are shown grayed out and will not be considered during the data analysis. Nevertheless, a temperature rise from seat row 2 till seat row 7 can be observed for both cases of MJV, see Fig. 8a and b. The data of 80 probes at chest level provide a maximum temperature difference of $\Delta \langle T \rangle_{chest} = 2.2$ K (maximum at seat 8 J $= 25.0$ °C and minimum at seat 2F $= 22.8$ °C) for the cruise scenario of MJV.
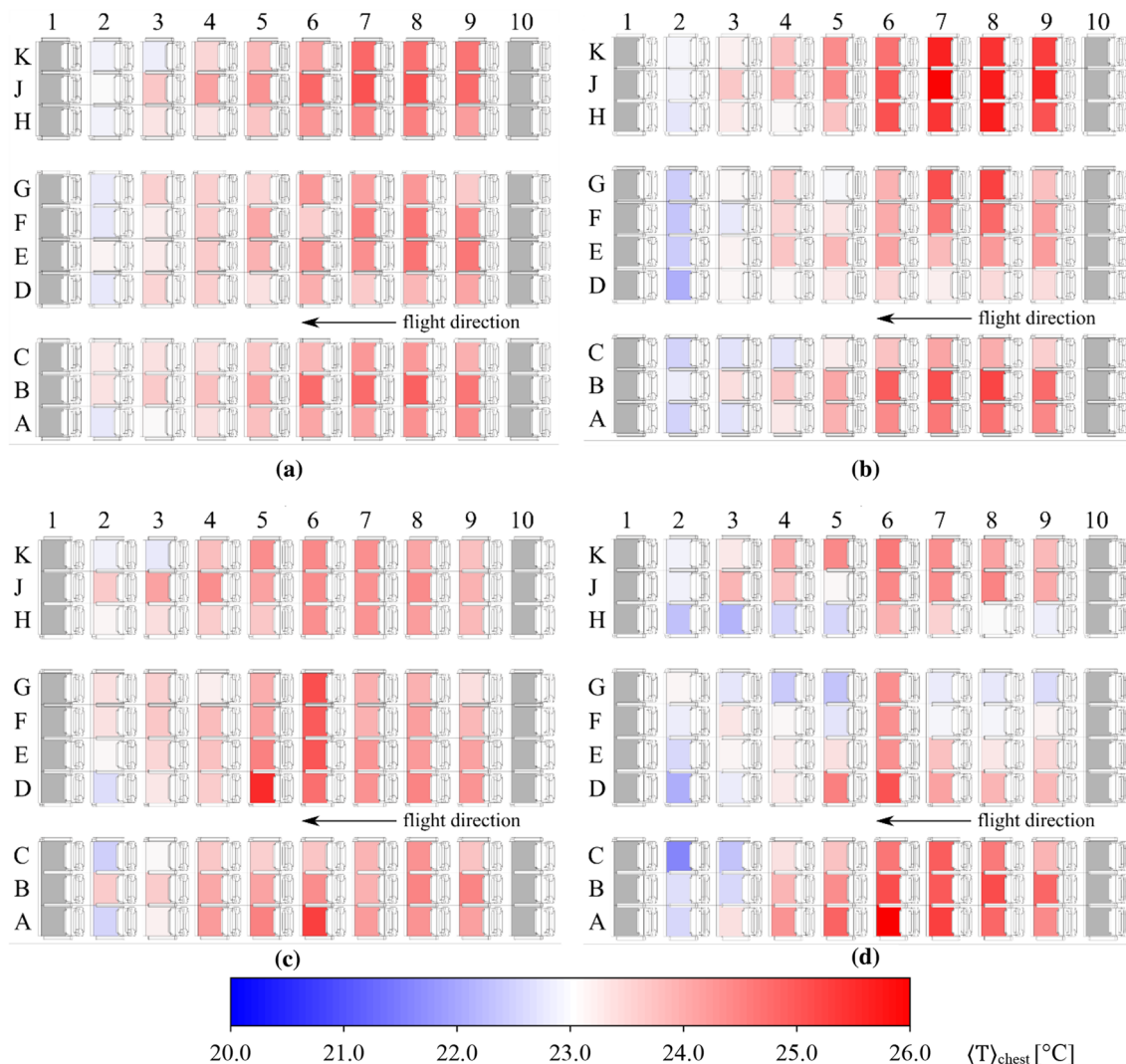

Fig. 8 Temperature distribution within the cabin measured at chest level in front of the TMs for MJV under cruise (**a**) and HDoG (**b**) conditions as well as for MV under cruise (**c**) and HDoG (**d**) conditions

Under HDoG conditions at MJV, the value increases by 77% to $\Delta \langle T \rangle_{chest} = 3.9$ K (maximum at seat 7 J = 26.0 °C and minimum at seat 2D = 22.1 °C). The temperature homogeneity of the data shown in Fig. 8a is characterized by a standard deviation (calculated for the 80 investigated seats) of 0.59 K for cruise conditions, whereas a value of 0.94 K is calculated for MJV under HDoG conditions, see Fig. 8b.

In contrast, the MV system provides a more inhomogeneous temperature distribution under both considered boundary conditions, see Fig. 8c and d. Here, spots with significantly colder or warmer temperatures occurred. Especially for MV at HDoG, cold temperatures can be seen at the center seat positions in the front and rear end of the cabin. For MV under cruise conditions, a maximum temperature difference of $\Delta \langle T \rangle_{chest} = 3.0$ K is determined. In this respect, the highest temperature of 25.5 °C is measured at seat 5D, while the lowest temperature occurred at seat 2C. The study for MV under HDoG provides a maximum temperature difference of $\Delta \langle T \rangle_{chest} = 5.2$ K (maximum at seat A6 = 26.8 °C and minimum at seat C2 = 21.6 °C), which is almost twice as high compared to cruise conditions. However, considering the standard deviation, calculated over the 80 data spots, MV performs equally as MJV for both thermodynamic conditions. At MV under cruise, the value amounts to 0.58 K and under HDoG a standard deviation of 0.92 K is determined.

Figure 9a and b show the mean fluid temperatures in the vicinity of the TMs at four height levels (ankle, knee, chest, head), measured with SR1 (see Fig. 6a) for MJV of both studied scenarios (cruise and HDoG). The first thing to note for both scenarios is, that the temperature distributions are very homogeneous for all height positions characterized by deviations of less than ± 1 K. To determine the temperature stratification occurring for these cases, the difference between time averaged head and ankle temperatures (ΔT_{h-a}) were evaluated for each seat position at SR1 (corresponds to seat row 4). The analyze reveals a maximum temperature stratification of $\Delta T_{h-a}^{max} = 3.4$ K at seat number 4B and $\Delta T_{h-a}^{max} = 1.5$ K at seat 4A for the cruise and HDoG scenario at MJV, respectively. The mean temperature stratification (spatial-averaged for all seat positions at SR1) between head and ankle position ($\langle \Delta T_{h-a} \rangle$) amounts 2.8 K under cruise conditions and 0.8 K for the HDoG case. Consequently, an operation range of roughly 2.0 K can be detected for both investigated cases, whereas each measured maximum temperature stratification is rated as not comfort-critical according to [30]. For MJV, the results of the fluid temperature measurements in the aisle, time-averaged over 1800s, are depicted in Fig. 9c). In this context, the cruise case shines out with a significant temperature stratification up to a height level of 85 cm, whereas
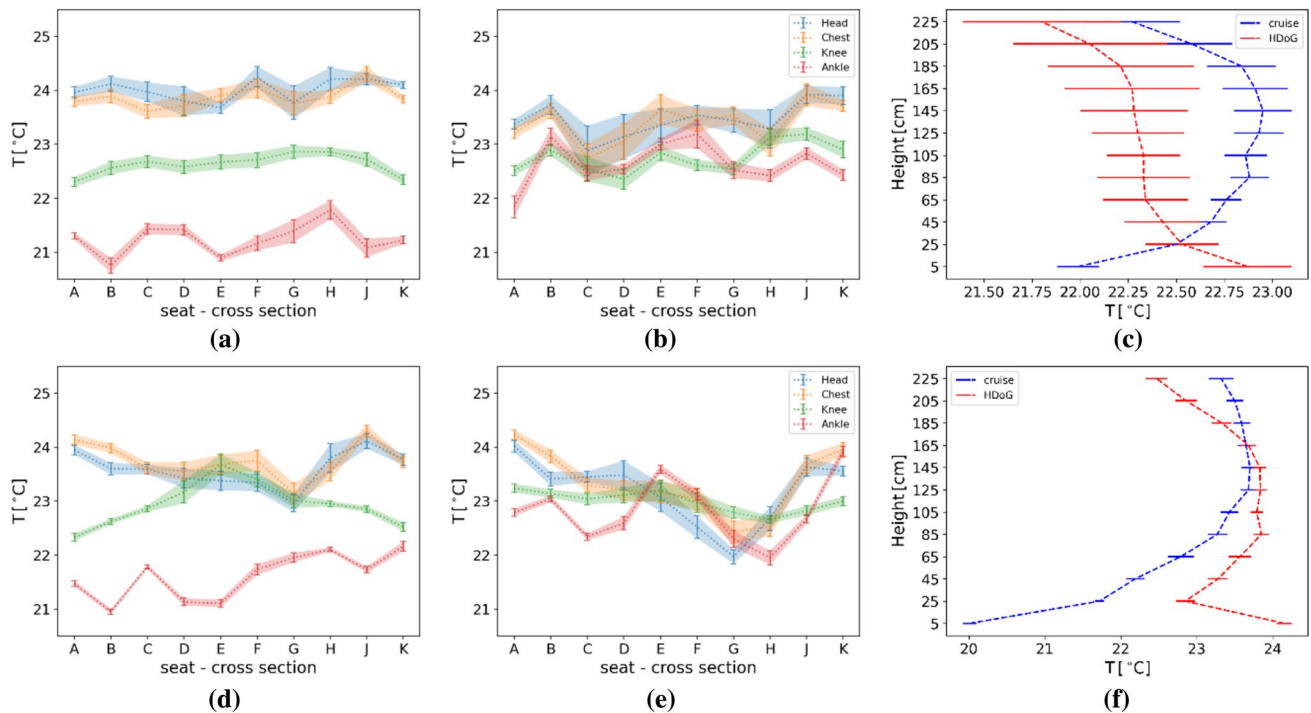
Fig. 9 Comparison of fluid temperatures. Temperature data in the vicinity of the TMs at four different height levels measured with SR1 for MJV at cruise (**a**) and "HDoG" (**b**) as well as for MV at cruise (**d**) and HDoG (**e**) conditions. **c** and **f** depict fluid temperatures measured in the aisle with SR3 for MJV and MV, respectively

the lowest measurement position is influenced by the temperature-controlled floor ($T_{gap} = 10.5$ °C during cruise scenario), causing this strong temperature gradient. After rather constant temperatures in the intermediate heights up to 165 cm, the temperature decreases in the upper part of the cabin. This results in a maximum temperature difference of 1.0 K and a mean standard deviation of 0.14 K. An inversed temperature stratification of 1.2 K from ceiling to floor level could be detected for MJV under HDoG conditions. Here, it is noticeable that high temperatures are measured near the ceiling (at height of 225 cm) although the inlet temperature is rather low with 12.4 °C. This suggests that either the incoming jet mixes quickly with the ambient air or that the supply air jets are deflected without passing the local sensor position in the center of the aisle. A mean standard deviation twice as high compared to cruise was found, however still below 0.6 K. The higher standard deviation under HDoG conditions might reflect a stronger fluctuation of the incoming air jets, possibly caused by the higher surface temperature gradient between floor and ceiling air exhaust and thus the higher thermal convective part of the flow. In comparison Fig. 9d and e show the corresponding mean fluid temperatures near the TMs (at the four different heights) for MV during cruise and HDoG scenario. The data for all measured heights reveal standard deviations of less than 0.5 K, which indicates only minor fluid temperature fluctuations and thus a very homogenous temperature distribution right in front of the manikins. While for MV at cruise

the maximum temperature stratification between head and ankle is $\Delta T_{h\text{-}a}^{max} = 2.6$ K (determined at seat 4B), the value is reduced by more than 50% to $\Delta T_{h\text{-}a}^{max} = 1.2$ K (calculated at seat 4A) for the HDoG case. Thus, the occurred temperature stratifications near the TMs for the MV system are also comfortable according to [30]. Regarding the temperature distribution in the aisle, Fig. 9f shows the time averaged data for MV under both thermodynamic conditions. Under cruise conditions, the temperature profile of MV is comparable to MJV characterized by lower temperatures in the lower cabin part (up to 85 cm) and only minor temperature stratifications at the remaining heights. For the HDoG case, some differences are determined. Here, a significant temperature drop of 1.3 K occurred between the lowest and the second lowest. Afterward the fluid temperature in the aisle increases to a height of about 100 cm and remains nearly constant above. At a height of 145 cm the temperature decreases again and reaches the lowest value of 22.5 °C near the ceiling. Here, the effect of the warm floor and rather cold ceiling area, due to the incoming fresh air, influence the temperature profile in the aisle. Summarizing the findings regarding T_{aisle}, the investigated cases are uncritical regarding thermal passenger comfort and are evaluated as comfortable according to [30].

To discuss the influence of the different ventilation techniques and different thermodynamic conditions on the surface temperatures, infrared images of the cabin interior are presented in Fig. 10. Generally, homogeneous surface temperatures in longitudinal direction of the cabin are
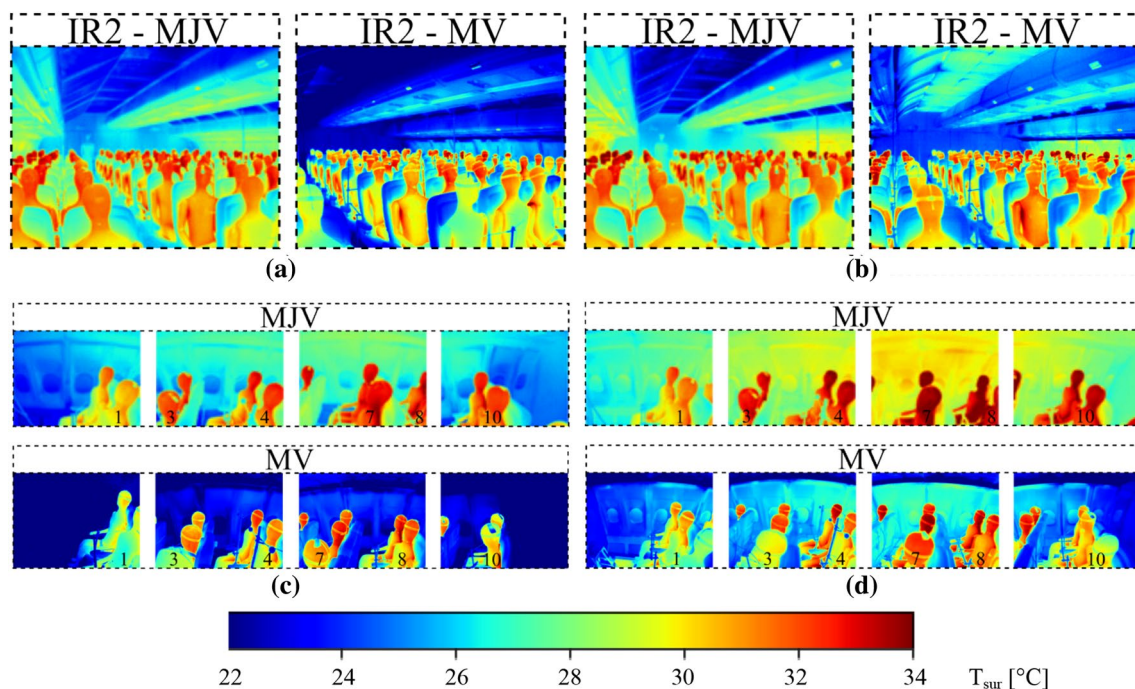
Fig. 10 Surface temperature distribution. Results for MJV and MV at cruise (**a**) and HDoG (**b**) conditions. Further, infrared images of the sidewall panels in FDR from seat row 1 (left) to 10 (right) are shown for cruise (**c**) and HDoG (**d**) conditions

observed. However, the surface temperatures of MV are significantly lower in comparison to MJV, independent of the analyzed boundary conditions. For both cruise and HDoG (see Fig. 10a and b), the surface temperatures of the TMs, sidewalls, overhead bins and seats are on average 3 K higher for MJV in contrast to MV, although T_{in} and T_{cab} of the two ventilation approaches is roughly the same at each considered case (see T_{in} in Table 3). The differences in surface temperatures reveal the changing relevance of forced convection on the heat transfer inside the cabin between both studied ventilation systems. Forced convection seems dominated at MV since the wall temperatures near the passengers are lower in comparison to MJV. Consequently, the thermal comfort is potentially improved for MJV due to the more comfortable surface temperatures of the inner sidewalls. As shown in Fig. 10a and b, the air outlet areas are clearly visible. At MJV under both conditions, the ceiling area is much colder than the remaining surfaces since the fresh air enters the cabin at this area. In contrast, the outlets above and below the lateral overhead bins are noticeable for MV. Here, the effect of the two different thermodynamic boundary conditions is also characterized by the surface temperatures at the ceiling linings, see MV in Fig. 10a and b. At cruise, the ceiling panels are significantly colder compared to HDoG. Figure 10c and d depict the surface temperature distribution at the inner sidewalls, exemplarily shown for the sidewall in FDR. Again, an impact of the boundary conditions in longitudinal flight direction is observed. However, an inhomogeneous temperature distribution is determined over the length of the cabin for both ventilation systems and both boundary conditions. Here, temperature differences at the inner sidewall of up to 6 K can be found even though the

gap temperatures are spatially constant at 10.5 ± 0.84 °C and 35.1 ± 0.48 °C for the cruise and HDoG cases. It is noticeable that the largest deviations occurred at the front and rear end of the cabin. We expect, that the boundary effects due to the missing heat loads in front of the first row as well as behind the last row also affect the resulting surface temperature distribution. As a result, the already slightly lower temperatures are even further reduced by increased downflow of cold air from the inlets, which is slightly shifted to these regions because of the missing rising warm plumes.

4.3 Fluid velocities

The flow velocities in the passenger zone are a further quantity to determine the passenger comfort.

Figure 11 depicts the fluid velocities measured in seat row 6 (see SR2 in Fig. 6a) at ankle, knee, chest and head level. Here, the data are time-averaged over 1800s and additionally spatially averaged over the ten seats (A to K) in the row. For the sake of clarity, the results are shown as boxplots with the mean value of all seats represented by the green dot. The data of MJV (solid lined boxes) and MV (dashed lined boxes) under cruise conditions are shown in subfigure a) while subfigure b) presents the mean fluid velocities for the two considered ventilation systems at the HDoG case. In general, for both conditions higher velocities are determined for MV at head and chest height due to the high momentum of the incoming air jets. At knee and ankle level, the velocities are equal or even lower for MV than for MJV. With regard to the mean velocities, the data for all seat positions in the corresponding seat row are characterized by a maximum value of 0.29 m/s for MV at cruise case, see Fig. 11a,
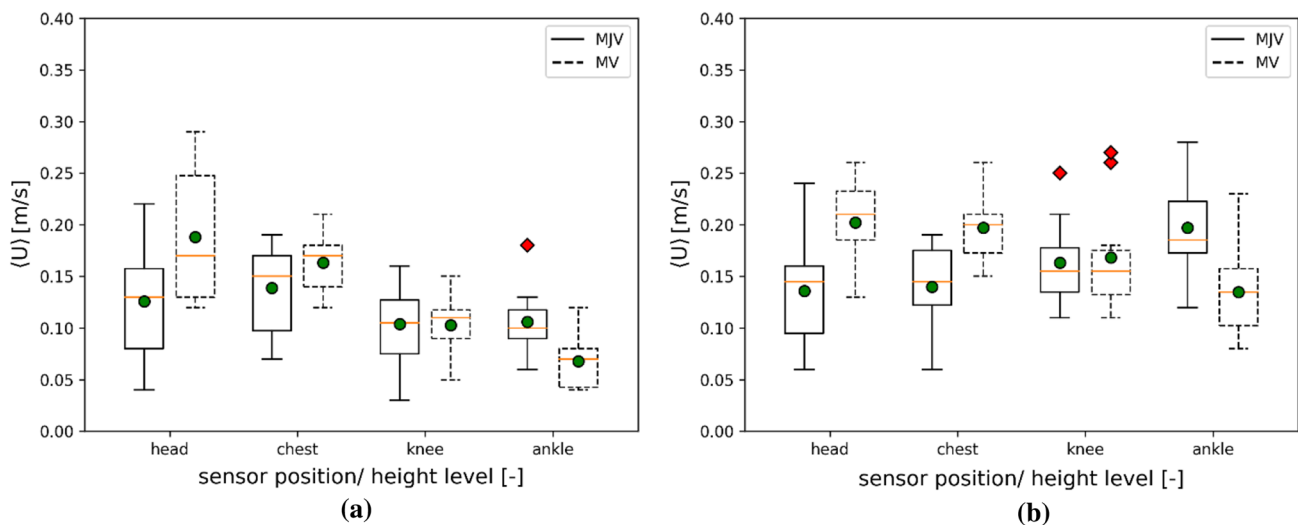
Fig. 11 Results of fluid velocities measured with SR2 at four different heights. (**a**) Data for MJV and MV under cruise conditions. (**b**) Data for MJV and MV under HDoG conditions. In this boxplot representation, the orange line marks the median, the green marker the mean value, the box the interquartile range and the outer markers the minimum/maximum value. Outliers are marked as red diamond

recorded at head level of seat position 6G. The highest value for MJV was measured at the same seat position and height level and amounts to 0.22 m/s. Based on the median velocities (orange lines), the values range from 0.11 m/s to 0.15 m/s for MJV and from 0.07 m/s to 0.17 m/s for MV, dependent on the considered body part. For the HDoG cases, the maximum velocity of 0.28 m/s was measured at ankle level of seat 6H for the MJV system, see Fig. 11b. When comparing the data between the two boundary conditions (cruise and HDoG), the measured velocities are slightly larger under HDoG conditions for almost all positions. This is also confirmed by the median values of the corresponding body parts, which cover a range of 0.14 m/s to 0.19 m/s for MJV and of 0.14 m/s to 0.21 m/s for MV. Generally, these data of the fluid velocities correspond well with the findings of the flow visualization, previously discussed. A major amount of the supplied air is flown toward the center seat bench resulting in higher fluid velocities at both seats near to the aisle (seat position G and H).

Using the objective quantities measured with the OVTP installed in seat row 6 at SR2, the draft rate (DR) was calculated according to [31] considering the local temperature, velocity and turbulence level. The DR is a further index to quantify the achievable thermal passenger comfort and describes the percentage of people predicted to be bothered by draft. Figure 12 shows the results of the DR spatially averaged for the selected sensor positions and body parts, respectively. Here, the data for cruise conditions are depicted in blue, while the values for the HDoG case are shown in red. Further, the results of MJV are marked in solid filled bar charts and the DR for MV is highlighted in light transparent and hatched bars. At each studied position, the DR for the cruise case is lower compared to the HDoG case for both MJV and MV. The comparison of the two ventilation systems reveals significantly

lower values for MJV than for MV at head, chest and knee level. At ankle height, however the DR of MV is lower compared to MJV. This finding corresponds with the fluid velocity data at ankle level. Here, higher velocities are observed for MJV. At MJV during cruise condition, the mean DR stays well below 10% with a maximum value of 8.2% measured at the chest region. In contrast, for HDoG conditions the mean DR of MJV exceeds the 10% value at the lower body parts (knee and ankle). Here, a maximum of 13.8% occurred at ankle height. Since the air temperatures on ankle level are higher for HDoG compared to cruise, the increased draft rate must be a result of the higher flow velocities (see Fig. 11) and potentially also of the higher turbulence intensity. On the other hand, the mean DR is higher than 10% for MV under cruise conditions at head and chest level characterized by a maximum value of 16.9% measured at head region, see the blue hatched bars in Fig. 12. Even higher values are observed for MV under HDoG conditions, where the 10% mark is exceeded at each measurement position (chest, head, knee and ankle). Here, the maximum DR amounts to 17.4% and is acquired at head region. In general, the higher DR for MV compared to MJV for the upper body parts are caused by the high inflow momentum of the fresh air below and above the lateral overhead bins. The higher DR at ankle level for MJV could be a result of recirculation effects near floor level.

4.4 Heat-removal-efficiency (HRE)

Finally, the heat removal efficiency (HRE) is determined and considered. It is defined in Eq. (1) with the air supply (T_{in}) and air exhaust (T_{out}) temperature as well as the mean temperature within the cabin (T_{cab}). Generally, the HRE is a measure how efficiently heat is removed from a room (with internal heat sources) by the ventilation system.

Equation (1): Definition of Heat Removal Efficiency (HRE)

$$HRE = 0.5 \cdot \left(T_{out} - T_{in} \right) \cdot \left(T_{cab} - T_{in} \right)^{-1} \qquad (1)$$

Based on this mathematical definition, the HRE is calculated for the four studied cases and summarized in Table 4.

Under cruise conditions, MJV and MV provide a HRE of 0.28 and 0.29, respectively. Both values are significantly lower than the theoretically possible value for MV (HRE = 0.5). Those low values are surprising since the temperature difference between T_{in} and T_{cab} is rather small. Here, it seems that a significant amount of heat disappears through the tempered fuselage elements, especially through the sidewalls. To test
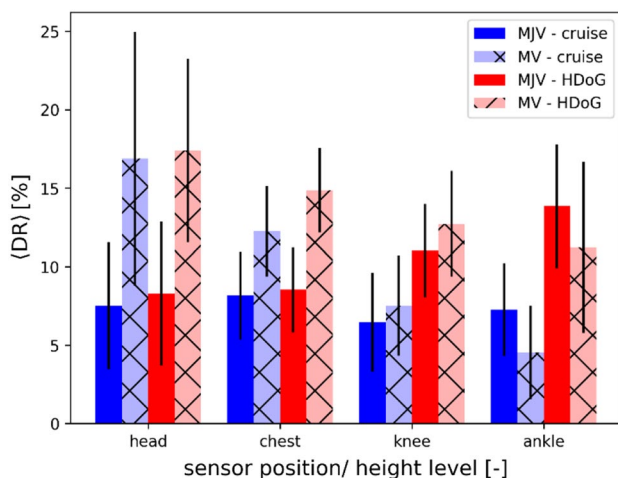
Fig. 12 Results of the mean Draft Rate for the studied height levels measured at SR2 in seat row 6

Table 4 Results of the heat removal efficiency for the studied cases

	MJV cruise	MJV HDoG	MV cruise	MV HDoG
HRE [−]	0.28	0.47	0.29	0.49

this hypothesis, a first estimation based on an energy balance was conducted which include the heat emission of the TMs (P_{TM}), the heat removal due to the enthalpy flow (P_V) and the dissipated heat through the surrounding areas (P_S), i.e., fuselage elements. The estimated energy balance is exemplified in Eq. (2).

Equation (2): Energy balance of the mock-up.

$$P_{TM} = P_V + P_S \tag{2}$$

During the experimental studies, each TM emits an average of 82 W of heating power. Thus, using 100 TMs results in a total amount of emitted heating power of $P_{TM} = 8.2$ kW. By means of air supply and air exhaust temperatures, the heating power dissipated by the enthalpy flow can be determined—exemplarily for the MJV case under cruise conditions—as followed (using parameters of air at 23°C = T_{cab}):

Equation 3: Heat removal through enthalpy flow.

$$P_V = \rho \cdot c_p \cdot \Delta T \cdot Q_v = 1.18 \frac{kg}{m^3} \cdot 1007 \frac{J}{kgK} \cdot$$
$$(20.8 - 18.0)K \cdot 1\frac{m^3}{s} = 3.33 \text{ kW} \tag{3}$$

Hence, only less than the half of the emitted heat is removed via the enthalpy flow. For MJV under cruise conditions, the major amount of approximately 4.9 kW of the released heat is transported through the fuselage elements. The cabin geometry benefits from this effect, since the sidewalls are rather large. A similar value of $P_V = 3.34$ kW is calculated for MV under cruise conditions. Accordingly, also in this case, most of the heat disappears through the fuselage elements. That explains the small values of HRE for both ventilation systems at the cruise case.

The evaluation of the heat removal efficiency under HDoG conditions shows a different picture with values of 0.47 and 0.49 (for MJV and MV). Applying Eq. 3) to the HDoG scenarios with a temperature difference of 10.1 K resp. 9.8 K (for MJV and MV) provide heat output of 12.0 kW and 11.6 kW. These are the heat quantities, which are removed via the ventilation system. Consequently, the warmer fuselage elements during these cases provide an additional heat load. As a result, a larger amount of heat is removed by the ventilation system. At this point we want to remark, that the calculation of the HRE is expected to strongly depend on the surface temperature of the floor. Two points support this assumption, firstly, the floor in the mock-up has a size of almost 70 m² and is operated at rather low temperatures. Here the same gap temperature is applied as at the side walls, however, only normal carpet serves as insulation layer and thus, the surface temperatures of the floor are cold compared to the inner side walls. Accordingly, we expect a large effect of the applied temperature boundary condition of the floor to the HRE. This highly interesting point will be subject of upcoming tests. The second point to note is the fact, that the exhaust openings are located directly above the floor in the position of the Dado panels. Hence, the temperature of the outflowing air, which is used for the calculation of the HRE, is strongly influenced due to the vicinity of the cold floor. Due to this – not jet fully investigated – impact of the floor temperature on the HRE, we waive to discuss the HRE results in the discussions section, where all other quantities are evaluated using a color code.

4.5 Comfort relevant parameters

Using the comfort sense system described in Sect. 3.1, evaluation of the thermal comfort near the passenger on seat 6J (Fig. 6a) was conducted by means of the PMV and PPD index. The PMV is a comfort index which reflects the human response to the local thermal environment. The thermal passenger comfort is rated from cold via neutral to warm by means of a 7-point scale ranging from -3 to + 3 [31]. The PPD index is related to the PMV values and provides a quantitative prediction of the percentage of thermally dissatisfied passengers, which feel too cool or too warm [31]. The measured and calculated values for different height levels are summarized in Table 5. A detailed view shows slight differences at four height levels irrespective of the studied case. In general, a better rating for MJV compared to MV is found at both conditions, cruise and HDoG. The mean PMV value (spatially averaged over the 4 height levels) measured during cruise conditions amounts to − 0.8 for MJV and − 1.1 for

Table 5 PMV and PPD values at seat position 6J at different heights for MJV and MV under cruise and HDoG conditions. The mean values, spatially averaged over all height levels, are given in the last line

	PMV				PPD [%]			
	Cruise		HDoG		Cruise		HDoG	
	MJV	MV	MJV	MV	MJV	MV	MJV	MV
Head	− 0.7	− 1.0	− 0.4	− 0.9	15.6	27.5	8.1	21.9
Chest	− 0.9	− 1.2	− 0.5	− 1.1	20.6	33.8	9.8	30.2
Knee	− 0.7	− 0.9	− 0.5	− 0.9	15.9	22.7	10.0	21.9
Ankle	− 0.9	− 1.1	− 0.6	− 1.0	20.9	29.9	13.8	25.8
Mean	**− 0.8**	**− 1.1**	**− 0.5**	**− 1.0**	**18.3**	**28.5**	**10.4**	**25.0**

MV. The other studied thermodynamic condition (HDoG) is characterized by higher temperatures at the fuselage elements, which significantly affect the measured PMV values. While for MJV a mean PMV index of − 0.5 is calculated, the mean value for MV under HDoG is twice as high, i.e., -1.0. On basis of the measured PMV values, PPD quantities were calculated as defined in [31]. PPD values lower than 21% are calculated at the different heights for MJV under both studied conditions. For MJV, resulting mean PPD values of 18.3% are calculated under cruise conditions and 10.4% is determined at HDoG case. In contrast, the PPD index increases for MV. A mean PPD value of 28.5% is found for the cruise case, whereas the percentage of thermally dissatisfied passenger is a little lower under HDoG conditions (25.0%). Consequently, the thermal comfort at seat 6J is significantly better during HDoG conditions for the MJV system. For MV on the other hand, the thermal comfort rating based on the PPD and PMV values is approximately the same for both conditions (cruise and HDoG). Furthermore, the MJV approach performs significantly better than the MV approach.

5 Discussion

With the objective to compare both ventilation scenarios and to identify a promising ventilation concept it is important to score the evaluation parameters, especially in terms of thermal passenger comfort. Based on the evaluation parameters given in Table 2, the following quantities are considered: the horizontal temperature homogeneity ($\Delta \langle T \rangle_{chest}$) calculated with the maximum and minimum temperature values at chest level of 80 RTDs, the vertical temperature stratification per seat position (in row 4) based on the maximum difference between time averaged head and ankle temperatures (ΔT_{h-a}^{max}) and the maximum (U_{max}) fluid velocities.

Further, the spatial averaged comfort-relevant indices of PMV and PPD are considered. The judgment criteria of the considered quantities are summarized in Table 6 and based either on thresholds given in the literature or on empirical values from previous measurement campaigns. Here, the limits of the fluid temperatures and velocities are in accordance with the data given in [30] while the interpretation for the PMV and PPD values follow the information given in [31]. Thereby, the evaluation criteria for PMV and PPD were specially defined in agreement with the project members to score ventilation systems. The thresholds for the DR also follow the values defined in the standards. For reasons of clarity and better identification, the scoring is visualized by means of color coding based on a traffic light color scheme.

Subsequently, the results presented in chapter 4 were rated in accordance with the previously introduced judgment criteria. The rating of the evaluation parameter is summarized in Table 7 for both ventilation system and both boundary conditions. The first parameter $\Delta \langle T \rangle_{chest}$ is an indicator for the horizontal temperature homogeneity within the cabin. For both cruise and HDoG conditions, the values are highlighted in yellow for MJV, which means that acceptable conditions are present. However, the value of $\Delta \langle T \rangle_{chest} = 3.9$ K for the HDoG scenario is only just in the judgment interval for acceptable conditions. In contrast, the values are higher for the MV system resulting in $\Delta \langle T \rangle_{chest} = 3.1$ K at cruise case, which is also rated as acceptable. However, during HDoG conditions the indicator for the horizontal temperature homogeneity increases to 5.1 K, which is rated as comfort critical. Here, the influence of the warm sidewalls significantly affects the temperature distribution measured at chest level of the TMs (see Fig. 8d), especially in the first half of the cabin. Hence, the horizontal temperature homogeneity is negatively affected resulting in a higher temperature difference between the maximum and minimum values, measured right in front of the TMs. The next quantity

Table 6 Judgment criteria of the comfort-relevant evaluation parameters

	critical	acceptable	comfortable
$\Delta \langle T \rangle_{chest}$	$\Delta \langle T \rangle_{chest} > 4$ K	2 K $< \Delta \langle T \rangle_{chest} \leq 4$ K	$\Delta \langle T \rangle_{chest} \leq 2$ K
ΔT_{h-a}^{max}	$\Delta T_{h-a}^{max} > 4$ K	2 K $< \Delta T_{h-a}^{max} \leq 4$ K	$\Delta T_{h-a}^{max} \leq 2$ K
U_{max}*	$U_{max} > 0.31$ m/s	0.16 m/s $< U_{max} \leq 0.31$ m/s	$U_{max} \leq 0.16$ m/s
DR	DR > 20 %	10 % $<$ DR ≤ 20 %	DR ≤ 10 %
PMV	PMV $> |0.8|$	$|0.5| <$ PMV $\leq |0.8|$	PMV $\leq |0.5|$
PPD	PPD > 20 %	10 % $<$ PPD ≤ 20 %	PPD ≤ 10 %

*Velocity thresholds are typically temperature dependent, here values for T≈23 °C, i.e., the mean temperature in the cabin, are given

Table 7 Rating of the evaluation parameter. *PMV and PPD values are only evaluated on seat position 6J

	$\Delta \langle T \rangle_{chest}$ [K]		ΔT_{h-a}^{max} [K]		$\langle U \rangle_{max}$ [m/s]		$\langle DR \rangle^{max}$ [%]		PMV* [-]		PPD* [%]	
	MJV	MV	MJV	MV	MJV	MV	MJV	MV	MJV	MV	MJV	MV
Cruise	2.2	3.1	3.4	2.6	0.22	0.29	8.2	16.9	-0.8	-1.1	18.3	28.5
HDoG	3.9	5.2	1.5	1.2	0.28	0.27	13.8	17.4	-0.5	-1.0	10.4	25.0

(ΔT_{h-a}^{max}) represents the maximum temperature stratification, which occurred near the TMs between head and ankle level at seat row 4.

For the cruise scenario, the evaluation parameters addressing the vertical temperature stratification are rated as acceptable for both MJV and MV. In this case, the gradient for MV is lower by 0.8 K than for MJV. At the HDoG scenario, MJV and MV provide comfortable conditions (highlighted in green) in terms of the vertical temperature stratification with values less than or equal to 1.5 K. Here again, MV performs slightly better than MJV, indicating a higher degree of mixing and thus a weaker temperature stratification. Furthermore, fluid velocities are also relevant for studies addressing thermal passenger comfort. For the rating, the maximum velocities ($\langle U \rangle_{max}$) are considered, which are acquired in seat row 4 at different height levels. The maximum velocities are scored as acceptable with values ranging from 0.22 m/s to 0.29 m/s for both studied ventilation systems (MJV and MV) under the two considered thermodynamic boundary conditions. For MJV, the maximum velocities are higher under HDoG conditions compared to the cruise scenario. One the other hand, the maximum value of MV at HDoG is lower than at cruise. However, for MV under both conditions, the measured maximum values are approximately the same within the limits of measurement accuracy. Nevertheless, all maximum values are lower than 0.31 m/s characterizing the limit for comfort-critical air velocities [30]. To evaluate the risk for air draft, the DR was also rated for the studied scenarios. For MJV during cruise, the mean values of the DR for all studied height levels are less than 10% characterized by a maximum of 8.2% at chest level, which results in a comfortable rating (representing the green color). The maximum DR is more than twice as high for MV (16.9%) at cruise compared to the corresponding MJV case. Thus, the limit of 10% is exceeded leading to an acceptable comfort rating (see yellow coloring in Table 7). For HDoG conditions, the values of $\langle DR \rangle^{max}$ are higher for both ventilation systems compared to the data at cruise conditions. Under these conditions (HDoG), the maximum value amounts to 13.8% for MJV, whereas at MV the value rises to 17.4%. However, in accordance with the rating given in Table 6, the DRs at HDoG are considered as still acceptable (representing yellow coloring in Table 7). However, considering the two comfort indices (PMV and PPD), which combine multiple comfort-relevant quantities, such as fluid temperature, air velocity and humidity, they are rated as comfort-critical for both MV cases (cruise and HDoG). Here, MV reveal PMV values larger or equal to -1.0 for the cruise and the HDoG scenario, respectively. These values exceed the limits for an acceptable comfort rating according to Table 6 and is therefore scored as comfort-critical characterized by a red color coding. It seems that the high inflow momentum at MV leads to higher fluid velocities

and a higher turbulence level, resulting in the corresponding PMV values. In contrast to MV, MJV shines out with lower PMV values. Under cruise conditions, the value amounts -0.8, which is just within the acceptable range (highlighted in yellow). Actually, a comfortable rating, denoted by green background color, was found for the HDoG scenario at MJV with a value of -0.5. However, this also borders on the range of acceptable conditions. The corresponding PPD values amount to 18% and 10% for MJV under cruise and HDoG conditions, respectively. Thus, the color coding is similar to the PMV values. That means for MJV, that only 18% of the passengers during cruise conditions are dissatisfied addressing the thermal conditions, while during HDoG just 10% of the passengers feel uncomfortable by the thermal conditions within the cabin. The reference cases with MV as a ventilation system provide PPD values of 28.5% and 25.0% at cruise and HDoG scenario, respectively. For these cases, the limit of 20% dissatisfied passengers is clearly exceeded. Hence, the PPD values are rated as comfort-critical and highlighted in red. It should be noted, that the PMV/PPD comfort assessment was only conducted on one seat (6J), hence its interpretation for the full cabin must be considered with care. For the selected seat, all PMV values were below zero, thus, an increase on the cabin temperature would result in even better evaluations. However, for the upcoming measurements other seats will be investigated regarding those two comfort quantities (PMV/PPD) to evaluate a more holistic rating of the thermal comfort.

6 Conclusions and outlook

Within the scope of the CleanSky 2 Joint Undertaking ADVENT, a new modular cabin mock-up was developed and set up at the DLR in Göttingen. This ground-based test bench is used for the experimental investigation of novel and innovative ventilation concepts in passenger compartments of aircraft addressing the topics of passenger comfort and energy efficiency, thus being directly in-line with the CO_2-fingerprint reduction goals of the EU. The new cabin mock-up reproduces the geometrical constraints of a passenger cabin on a 1:1 scale, typical for modern long-range airliners. Further it enables experimental studies under realistic thermodynamic boundary conditions by means of temperature-controlled fuselage elements. Herewith, different operational and flight phases can be simulated experimentally covering relevant temperature ranges and time scales. This was validated with experimental data acquired during flight tests with an A320. In addition, due to the modular design approach, the mock-up provides a high flexibility regarding the installation of new ventilation concepts and the corresponding novel cabin air inlets. The latter also benefits

the installation of different cabin geometries (e.g., short- and middle-range cabin geometries) and other seating layouts.

For the present study, a novel ventilation approach was installed and analyzed based on the air supply through micro-jet air inlets mounted at the ceiling in the aisle. Here, the air enters the cabin via numerous jets with a rather high momentum. After mixing of cabin air with fresh air, the air leaves the cabin through openings at floor level, which are located near the Dado panels. In addition, the novel ventilation concept was compared with a generic version of a mixing ventilation, which is state-of-the-art for air conditioning in an aircraft. Both concepts are studied for two different operational cases cruise and hot-day-on-ground to evaluate the performance of the ventilation systems under different boundary conditions. Besides the qualitative analysis of the flow pattern, a dedicated cabin measurement installation was used to capture flow velocities, fluid and surface temperatures at previously defined locations. The simulation of the heat impact caused by the passengers is realized using thermal manikins. In the vicinity of the manikins as well as in the aisle, temperature and velocity stratifications were captured. Comfort relevant quantities, such as predicted mean vote and percentage of dissatisfied passengers, were measured and calculated. Further, the performance of the ventilation approach for removing heat loads were evaluated for both studied cases.

The results regarding the evaluation of the micro-jet ventilation as a novel concept identified both the potential and the challenges of the system. However, especially in comparison with the generic mixing ventilation, the new concept provides comfortable thermal conditions, which are comparable or even better.

Except of the first and last seat row, where boundary effects occur, the spatial homogeneity of the fluid temperature in horizontal direction is promising for the new concept and below comfort-critical thresholds. Here, the maximum deviations are significantly lower compared to the mixing ventilation approach. Considering the vertical temperature stratification near the manikins, the novel ventilation systems performs slightly worse than the reference case. However, the occurred maximum temperature difference are not comfort-critical and rated as acceptable or even comfortable, dependent on the considered boundary conditions. The fluid velocities are generally very low on most of the seats. The new concept provides maximum velocities, which are equal within the measurement accuracy. Regarding the maximum measured draft rate, the micro-jet ventilation system is still lower than 14%, while for the mixing ventilation even higher percentages occurred. This is also confirmed by the

evaluation of the comfort parameters. Depending on the considered thermodynamic boundary conditions, a maximum of 18% of the passengers are dissatisfied with the thermal conditions. In contrast, this value rises to over 28% for the generic mixing ventilation concept. This brief evaluation of the micro-jet ventilation concept has identified that smaller modifications regarding the supply air configuration and a re-positioning of the exhaust openings could already fulfill all requested thresholds. Finally, it should be noted, that such a ceiling-integrated ventilation concept is also beneficiary regarding pipe lengths and installation effort.

As an outlook, the installed micro-jet-ventilation system will be studied in detail by further measurements. First, the installed measurement system will be enhanced by a multi-gas monitoring system to determine the air quality for the considered ventilation system. In addition, experimental studies under dynamic and transient thermodynamic boundary conditions will be addressed. The variation of the volume flow rates, the flow distribution as well as measurements with variation in the heat load emission is also scheduled to identify drawbacks and optimization potential. Regarding the evaluation of the HRE, a strong impact of the floor temperature was determined. Hence, in further studies the effect of this temperature and the positioning of the exhaust openings will be studied in detail. All results will flow into a validation data matrix as defined in the scope of the underlying ADVENT project.

Declarations

Conflict of interest The authors have no competing interests to declare that are relevant to the content of this article.

References

1. IATA - International Air Transport Association: "A global approach to reducing aviation emissions. First stop: carbon-neutral growth from 2020," Montreal, Canada

2. European Commission: "The European Green Deal COM 640," 2019. [Online]. Available: https://eur-lex.europa.eu/resource.html?uri=cellar:b828d165-1c22-11ea-8c1f-01aa75ed71a1.0002.02/DOC_1&format=PDF. Accessed 29 June 2021

3. Martinez, I.: "Aircraft Environmental Control," P.U.o. Madrid, Madrid, Spain, 2014.

4. Knepple, R. A.: "The Energy-Autonomous Cabin - The End of Classical On-Board Power Supply?," in *4th International Workshop on Aircraft System Technologies*, Hamburg, 2013.

5. A^3 by Airbus LLC, "Transpose project," 2018 March 2018. [Online]. Available: https://acubed.airbus.com/projects/transpose/. Accessed 24 Feb 2021

6. Newsweek Digital LLC, "Newsweek," 12th December 2016. [Online]. Available: https://www.newsweek.com/airbus-imagines-planes-future-will-be-modular-531744. Accessed 24 Feb 2021

7. Elmaghraby, H.A., Chiang, Y.W., Aliabadi, A.A.: Ventilation strategies and air quality management in passenger aircraft cabins: a review of experimental approaches and numerical simulations. Sci Technol Built Environ **24**(2), 160–175 (2018). https://doi.org/10.1080/23744731.2017.1387463

8. Schmidt, M., Gores, I., Markwart, M.: Numerical study of different air distribution systems for aircraft cabins. Technical University of Denmark, Denmark (2008)

9. Zhang, C.: Novel air distribution systems for commercial aircraft cabins. Build. Environ. **42**(4), 1675–1684 (2007). https://doi.org/10.1016/j.buildenv.2006.02.014

10. Zhang, T., Li, P., Zhao, Y., Wang, S.: Various air distribution modes on commercial airplanes - Part 2: computional fluid dynamics modeling and validation. HVACR Res. **19**(5), 457–470 (2013)

11. Bosbach, J., Heider, A., Dehne, T., Markwart, M., Gores, I., Brendfeldt, P.: Flight testing of alternative ventilation systems for aircraft cabins. In: New results in numerical and experimental fluid mechanics IX, pp. 275–283. Springer International Publishing (2014)

12. Bosbach, J., Heider, A., Dehne, T., Markwart, M., Gores, I., Bendfeldt, P.: Evaluation of cabin displacement ventilation under flight conditions. 28th International Congress of the Aeronautical Sciences ICAS2012, Brisbane, Australia (2012)

13. Dehne, T., Bosbach, J., Heider, A.: Comparison of surface temperatures and cooling rates for different ventilation concepts in an A320 aircraft cabin under flight conditions." In: 13th SCANVAC International Conference on Air Distribution in Rooms and Airplanes, Sao Pauo, Brazil, (2014)

14. Bosbach, J.: Alternative ventilation concepts for aircraft cabins. CEAS Aeronaut. J. **4**, 301–313 (2013). https://doi.org/10.1007/s13272-013-0074-z

15. Müller, D., Schmidt, M., Müller, B.: Application of displacement ventilation systems for air flow distribution in aircraft cabins. AST, Hamburg, Germany (2011)

16. Zhang, T., Li, P., Zhao, Y., Wang, S.: Various air distribution modes on commercial airplanes. Part 1: experimental measurements. HVACR Res. **19**(3), 268–282 (2013)

17. Yan, W., Zhang, Y., Sun, Y., Li, D.: Experimental and CFD study of unsteady airbone pollutant transport within aircraft cabin mock-up. Build. Environ. **44**(1), 34–43 (2009). https://doi.org/10.1016/j.buildenv.2008.01.010

18. Zhang, Z., Chen, X., Mazumdar, S., Zhang, T., Chen, Q.: Experimental and numerical investigation of airflow and contaminant transport in an airliner cabin mock-up. Build. Environ. **44**(1), 85–94 (2009). https://doi.org/10.1016/j.buildenv.2008.01.012

19. Li, B., Duan, R., Li, J., Huang, Y., Yin, H., Lin, C.-H., Wei, D., Shen, X., Liu, J., Chen, Q.: Experimental studies of thermal environment and contaminant transport in a commercial aircraft cabin with gaspers on. Indoor Air **26**(5), 806–819 (2016). https://doi.org/10.1111/ina.12265

20. Zhu, X., Liu, J., Cao, X., Li, J.: 2D-PIV experimental study on the air distribution with natural convection effect of passengers in an air cabin mockup. Procedia Eng. **121**, 866–874 (2015). https://doi.org/10.1016/j.proeng.2015.09.041

21. Li, J., Cao, X., Liu, J., Wang, C., Zhang, Y.: Global airflow field distribution in a cabin mock-up measured via large-scale 2D-PIV. Build. Environ. **93**, 234–244 (2015). https://doi.org/10.1016/j.buildenv.2015.06.030

22. Pathak, A., Norrefeldt, V., Pschirer, M.: Validation of a simulation tool for an environmentally freindly aircraft cargo fire protection system. Aerospace J. **8**(2), 35 (2021). https://doi.org/10.1088/1757-899X/1024/1/012091

23. German Aerospace Center (DLR), "Modular Cabin Mock-up Gottingen (MKG)," 2019. [Online]. Available: https://www.dlr.de/content/en/research-facilities/modular-cabin-mock-up-goettingen-mkg.html. Accessed 1 Apr 2021

24. German Aerospace Center (DLR), "CENT - Comfort and efficiency enhancing technologies," Unpublished internal company report, Göttingen (2017)

25. Norrefeldt, V., Riedl, G.: Investigation of the impact of a particle foam insulation on airflow, temperature distribution, pressure profile and frost buildup on the aircraft structure. Aerospace **8**(12), 359 (2021). https://doi.org/10.3390/aerospace8120359

26. Elmaghraby, H.A., Chiang, Y.W., Aliabadi, A.A.: Normal and extreme aircraft accelerations and the effects on exposure to expiratory airborne contaminant inside commercial aircraft cabins. Sci. Technol. Built Environ. **26**(7), 924–927 (2020). https://doi.org/10.1080/23744731.2020.1771808

27. Sensirion A.G.: "Differential pressure sensors," Sensirion - The sensor company, [Online]. Available: https://www.sensirion.com/fileadmin/user_upload/customers/sensirion/Dokumente/8_Differential_Pressure/Datasheets/Sensirion_Differential_Pressure_Datasheet_SDP8xx_Digital.pdf. Accessed 23 Mar 2021

28. Schmeling, D., Volkmann, A.: On the experimental investigation of novel low-momentum ventilation concepts for cooling operation in a train compartment. Build. Environ. **182**, 107–116 (2020). https://doi.org/10.1016/j.buildenv.2020.107116

29. EN 13129:2016, "Railways Application; Air Conditioning for Main Line Rolling Stock, Comfort Parameters and Type Tests," European Committee for Standardization, Bruxelles (2016)

30. ASHRAE: "ASHRAE 2001 - handbook of fundamentals," p. 2001. American Society of Heating, Refrigeration and Air Conditiong Engineers Inc, , Atlanta (2001)

31. EN ISO 7730, "Ergonomics of the thermal environment - Analytical determination and interpretation of thermal comfort using calculation of the PMV and PPD indices and local thermal comfort criteria," European Commitee for Standardization , Bruxelles (2005)

32. Lange, P.: Planning and design of a cabin mopck-up in consideration of future long-range concepts. DLR - German Aerospace Center, Göttingen, Germany (2019)